2010

Apparent Seasonal Cycle in Isotopic Discrimination of Carbon in the Atmosphere and Biosphere Due to Vapor Pressure Deficit

Ashley P. Ballantyne
University of Montana - Missoula, ashley.ballantyne@umontana.edu

J. B. Miller

P. P. Tans

Apparent seasonal cycle in isotopic discrimination of carbon in the atmosphere and biosphere due to vapor pressure deficit

A. P. Ballantyne,[1,2] J. B. Miller,[1,3] and P. P. Tans[1]

Received 29 June 2009; revised 5 May 2010; accepted 24 May 2010; published 10 September 2010.

[1] We explore seasonal variability in isotopic fractionation by analyzing observational data from the atmosphere and the biosphere, as well as simulated data from a global model. Using simulated values of atmospheric CO_2 and its carbon isotopic composition, we evaluated different methods for specifying background concentrations when calculating the isotopic signature of source CO_2 (δ_s) to the atmosphere. Based on this evaluation, we determined that free troposphere measurements should be used when available as a background reference when calculating δ_s from boundary layer observations. We then estimate the seasonal distribution of δ_s from monthly climatologies derived from several atmospheric sampling sites. This approach yields significant seasonal variations in δ_s with more enriched values during the summer months that exceed the uncertainty of δ_s estimated for any given month. Intra-annual measurements of $\delta^{13}C$ in the cellulose of *Pinus taeda* growing in the southeastern U.S. also reveal seasonal isotopic variations that are consistent in phase but not necessarily amplitude with atmospherically derived estimates of δ_s. Coherent seasonal patterns in δ_s inferred from the atmosphere and observed in the biosphere were not consistent with the seasonal isotopic discrimination simulated by a commonly used biosphere model. However, δ_s seasonality consistent with observations from the atmosphere and biosphere was retrieved with a revised biosphere model when stomatal conductance, and thus isotopic discrimination, was allowed to vary in response to vapor pressure deficit rather than relative humidity. Therefore, in regions where vapor pressure deficit and relative humidity are positively covariant over the growth season, such as the sub-tropics, different stomatal conductance models may yield very different estimates of CO_2 and H_2O exchange between the biosphere and atmosphere.

Citation: Ballantyne, A. P., J. B. Miller, and P. P. Tans (2010), Apparent seasonal cycle in isotopic discrimination of carbon in the atmosphere and biosphere due to vapor pressure deficit, *Global Biogeochem. Cycles*, *24*, GB3018, doi:10.1029/2009GB003623.

1. Introduction

[2] One of the central challenges to understanding how Earth works as a system, is to better account for the transfer of carbon between the biosphere and the atmosphere [*Falkowski et al.*, 2000]. Although atmospheric CO_2 continues to increase at an unprecedented rate, about half of the fossil fuel emissions continue to be captured by the oceans or terrestrial biosphere [*Schimel et al.*, 2000]. However, identifying the location and magnitude of this carbon sink still eludes biogeochemists [*Schlesinger*, 2004]. This is due in part to local variability in fluxes and shifts in the partitioning of carbon between land and ocean reservoirs in response to climate variability [*Battle et al.*, 2000; *Bousquet et al.*, 2000]. One approach to constraining the global carbon budget is investigating the changes in the isotopic composition of CO_2 ($\delta^{13}CO_2$) over time to infer changes in sources and sinks of CO_2 to the atmosphere [*Battle et al.*, 2000; *Ciais et al.*, 1995].

[3] Because the terrestrial biosphere preferentially takes up the lighter ^{12}C isotope to a greater extent than the marine biosphere, measurements of $\delta^{13}CO_2$ have conventionally been used to partition carbon uptake between the land and ocean. The discrimination against the heavier isotope in CO_2 occurs primarily due to the enzymatic preference for the lighter isotope during carboxylation in C_3 plants ($\Delta_{al} \approx$ 18.0 ‰) and due to greater diffusivity of the lighter isotope in C_4 plants (Δ_{al} = 4.4 ‰), yielding global estimates of assimilation-weighted discrimination by the terrestrial biosphere between 14.8 ‰ and 16.5 ‰ [*Fung et al.*, 1997; *Lloyd and Farquhar*, 1994; *Suits et al.*, 2005]. In contrast to

[1]NOAA Earth Systems Research Laboratory, Boulder, Colorado, USA.
[2]Now at Geological Sciences Department, University of Colorado, Boulder, Colorado, USA.
[3]Cooperative Institute for Research in Environmental Science, University of Colorado, Boulder, Colorado, USA.

0886-6236/10/2009GB003623

the atmosphere-land net flux, the atmosphere-ocean net flux of CO_2 is associated with a fractionation that is approximately an order of magnitude less than the discrimination due to terrestrial photosynthesis ($\varepsilon_{ao} \approx -2.0$ ‰) [*Randerson*, 2005; *Zhang et al.*, 1995]. This difference between the relatively large isotopic discrimination by the land and the relatively small isotopic fractionation by oceans has allowed researchers to partition the amount of atmospheric carbon taken up between land and ocean sinks [*Battle et al.*, 2000; *Ciais et al.*, 1995]. However, most atmospheric inversion models assume that Δ_{al} is temporally invariant [*Battle et al.*, 2000; *Ciais et al.*, 1995; *Enting et al.*, 1995], despite emerging evidence that isotopic discrimination may change over a range of timescales.

[4] Recent studies of isotopic discrimination indicate that Δ_{al} may vary from seasonal to decadal time scales [*Conte and Weber*, 2002; *Randerson et al.*, 2001; *Scholze et al.*, 2003]. By measuring the $\delta^{13}C$ of leaf wax biomarkers in aerosols transported from N. America, *Conte and Weber* [2002] estimate a 5–6‰ seasonal cycle in the amplitude of Δ_{al} which they attribute to changes in primary productivity and the relative discrimination between C3 and C4 vegetation. On inter-annual timescales changes in Δ_{al} have been documented in response to climate variables associated with El Niño that are thought to impact the partitioning between marine and terrestrial carbon uptake [*Randerson et al.*, 2001]. Last, a study employing a dynamic global vegetation model found considerable inter-annual variability in Δ_{al} resulting in a 0.8 PgC yr^{-1} change in the inferred amount of carbon uptake by the terrestrial biosphere between years [*Scholze et al.*, 2003]. These studies suggest that isotopic discrimination may vary over a range of timescales but with uncertainty as to the sign and magnitude of variability.

[5] To a first approximation, a 1‰ decrease in Δ_{al} can result directly in a 0.1 to 0.4 PgC yr^{-1} increase in the inferred uptake of carbon by the terrestrial biosphere [*Still et al.*, 2003]. However, slight changes in Δ_{al} can also "indirectly" affect the inferred partitioning of the global carbon budget due to the isotopic disequilibrium between the biosphere and the atmosphere [*Randerson*, 2005]. This is because Δ_{al} is embedded in the terrestrial disequilibrium term of the global isotopic carbon budget and the gross flux of heterotrophic and autotrophic respiration represents such a large flux in the global carbon budget (see equations (5) and (6)). Thus a slight decrease in Δ_{al} of 0.1‰ can result in a disproportionately large change in terrestrial disequilibrium ultimately resulting in a 0.7 PgC yr^{-1} increase in the inferred terrestrial carbon sink. Therefore, slight changes in Δ_{al} over a range of timescales can result in significant uncertainties in the partitioning of the global carbon budget between land and ocean sinks.

[6] Ultimately, we would like to make inferences based on atmospheric measurements about processes that govern the global carbon budget [*Battle et al.*, 2000; *Ciais et al.*, 1995; *Tans et al.*, 1990]. This has been done with some success at local scales by analyzing the $\delta^{13}C$ of respired CO_2 collected below the canopies of forested ecosystems at night using the Keeling plot approach [*Flanagan et al.*, 1996; *Keeling*, 1958; *Pataki et al.*, 2003]. Similar attempts to infer isotopic discrimination due to terrestrial processes have been made from atmospheric measurements at regional to continental scales [*Bakwin et al.*, 1998]; however, it is quite difficult to differentiate the influences of terrestrial, marine and fossil fuel fluxes on atmospheric measurements. *Bakwin et al.* [1998] used measurements of CO_2 and $\delta^{13}CO_2$ in combination with CO measurements from a global distribution of sites to distinguish fossil fuel fluxes from terrestrial biosphere fluxes, but oceanic fluxes could not be neglected at sites near marine sources. *Pataki et al.* [2006] used a similar approach to deduce that as much as 60–70% of urban emissions were derived from natural gas, but the influence of terrestrial and marine fluxes on background concentrations were assumed to be negligible.

[7] Here we use an alternative approach to the Keeling plot [*Miller and Tans*, 2003] to explore seasonal changes in the isotopic signature of CO_2 sources (δ_s) to the atmosphere. We then use the simple biosphere model (SiB 2.5) to identify the optimal background reference curve for calculating δ_s. Seasonal variations in δ_s inferred from atmospheric measurements are then compared to in situ measurements of seasonal isotopic variability in tree ring cellulose. Last, we use observations to evaluate key differences in stomatal conductance models that yield contradictory isotopic predictions and thus different estimates of carbon and water exchange between the biosphere and the atmosphere.

2. Theoretical Approach and Methods

2.1. Sources of Carbon to the Atmosphere: From the Keeling Plot to the Global Budget

[8] The relationship between CO_2 and its carbon isotopic composition was first identified by *Keeling* [1958], who exploited this relationship to identify the isotopic signature of CO_2 sources to the atmosphere. This approach is based on the conservation of mass, such that:

$$c_a = c_{bg} + c_s \tag{1}$$

where the atmospheric concentration of CO_2 (c_a) can be estimated from the sum of the background CO_2 concentration (c_{bg}) and the source CO_2 concentration (c_s). Because the product of CO_2 and its isotopic composition (δ), is effectively conserved [*Tans*, 1980], equation (1) can be rewritten as follows:

$$\delta_a c_a = \delta_{bg} c_{bg} + \delta_s c_s \tag{2}$$

to include the respective isotopic tracers of atmospheric (δ_a), background (δ_{bg}) and net source (δ_s) of CO_2. Equation (1) can then be substituted into equation (2) and manipulated to formulate the conventional Keeling plot where the y-intercept corresponds with δ_s. This approach has been widely used in ecosystem studies where it is assumed that δ_{bg} is constant [*Bakwin et al.*, 1998; *Bowling et al.*, 2002; *Flanagan et al.*, 1996; *Keeling*, 1958; *Pataki et al.*, 2003]. This constant background assumption is approximately valid when sampling respired air during the night in the absence of photosynthesis and atmospheric mixing. However, when sampling

well-mixed air in the troposphere during the day, especially over days to years, it is not valid to assume that δ_{bg} remains constant. Thus a permutation of the original Keeling plot has been proposed by *Miller and Tans* [2003]:

$$\delta_a c_a - \delta_{bg} c_{bg} = \delta_s (c_a - c_{bg}). \quad (3)$$

This approach allows us to specify background values of CO_2 and $\delta\,^{13}C$ that may vary with time. We may then calculate the differences between atmospheric observations of CO_2 and of the product of $\delta^{13}C$ and CO_2 and their corresponding background values. These differences, hereafter referred to as "residuals," can then be inserted into equation (3) and δ_s can be calculated by solving for the slope term. Although this approach allows us to infer changes in the source of CO_2 from atmospheric measurements on a regional scale, there are still numerous isotopic fluxes that have an impact on δ_s. Therefore, when estimating changes in the global CO_2 content of the atmosphere (C_a) we must consider the major fluxes to the atmosphere, such that:

$$\frac{dC_a}{dt} = F_f + N_l + N_o, \quad (4)$$

where F_f represents the flux from fossil fuels, N_l represents the net flux from land, and N_o represents the net flux from the ocean. These changes in fluxes to the atmosphere are accompanied by changes in the isotopic signature of source fluxes; thus, the global isotopic carbon budget can be written as (modified from *Tans et al.* [1993, p. 356, equation 16]):

$$\frac{d(\delta_a C_a)}{dt} = \delta_f F_f + N_l \delta_{al} + G_{la}(\delta_{la} - \delta_{al}) + N_o \delta_{ao} + G_{oa}(\delta_{oa} - \delta_{ao}), \quad (5)$$

where δ_f represents the isotopic signature of fluxes from fossil fuels, δ_{al} represents the isotopic signature caused by uptake of atmospheric CO_2 by the land and can be estimated as:

$$\delta_{al} = \delta_a - \Delta_{al} \quad (6)$$

and δ_{ao} represents the isotopic signature caused by uptake of atmospheric CO_2 by the ocean and can be estimated as:

$$\delta_{ao} = \delta_a + \varepsilon_{ao}. \quad (7)$$

In addition to the net fluxes, we must also consider the gross one-way carbon fluxes from the land to the atmosphere (G_{la}), from the ocean to the atmosphere (G_{oa}), and their associated isotopic disequilibria, where δ_{la} represents the isotopic signature of fluxes from the land to the atmosphere and δ_{oa} represents the isotopic signature of fluxes from the ocean to the atmosphere.

[9] Thus it is apparent that small changes in Δ_{al} can result in large changes in the inferred atmospheric carbon budget, directly through the N_l term and indirectly through the G_{la} term in equation (5). It is also apparent from this expanded isotopic carbon budget that values of δ_s inferred from atmospheric measurements do not necessarily reflect any single term in the global atmospheric budget, but rather a flux-weighted mean of all the terms in our atmospheric carbon budget, such that:

$$\delta_s = \frac{\delta_f F_f + N_l \delta_{al} + G_{la}(\delta_{la} - \delta_{al}) + N_o \delta_{ao} + G_{oa}(\delta_{oa} - \delta_{ao})}{F_f + N_l + G_{la} + N_o + G_{oa}}. \quad (8)$$

Although it is exceedingly difficult to assess how all of these terms influence the atmospheric carbon budget, here we rely on a global biosphere model combined with an atmospheric transport model to evaluate how each of these terms impacts our atmospheric measurements. While the disequilibrium fluxes are significant at annual to decadal timescales, they are relatively small compared to the net fluxes at monthly to seasonal timescales. Last, in order to isolate the isotopic signature of the terrestrial biosphere we focus our analysis on atmospheric sampling sites where fluxes are dominated by terrestrial processes with greatly reduced fossil fuel fluxes.

2.2. Atmospheric Observations of CO_2 and $\delta\,^{13}C$ at Sites in the Global Sampling Network

[10] For our inferences of seasonal sources of CO_2 to the atmosphere we focused on three North American sites from the NOAA/ESRL flask network (http://www.esrl.noaa.gov/gmd/ccgg/). These included two tall tower sites located at Park Falls, Wisconsin (LEF; 868 masl; 45.93° N, 90.27° W) and Grifton, North Carolina (ITN; 505 masl; 35.35° N, 77.38° W), as well as one surface sampling site at Wendover, Utah (UTA; 1320 masl; 39.90° N, 113.72° W). These sites were selected because they represent a range of North American ecosystems and they have been sampled continuously for CO_2 and $\delta\,^{13}C$ for at least 5 years. Although sampling at ITN was discontinued in 1999, the duration of the data coincide well with our isotopic measurements from pine trees growing in North Carolina (see below). Because atmospheric measurements at Niwot Ridge, Colorado (NWR; 3475 masl; 40.05° N, 105.58° W) are highly correlated with measurements of CO_2 ($R = 0.74$; p-value < 0.0001) and $\delta^{13}CO_2$ ($R = 0.66$; p-value < 0.0001) made in the free troposphere (2000 and 5000 masl) over North America, even when the annual trend is removed, NWR was selected as our background reference representative of the free troposphere.

2.3. Seasonal Measurements of $\delta\,^{13}C$ in Cellulose From Annual Growth Rings in Trees

[11] To test for seasonal variation in Δ_{al} due to the terrestrial biosphere, carbon isotopes were analyzed within the cellulose of tree cores. We extracted tree cores from 30 loblolly pines (*Pinus taeda*) growing in Duke Forest, NC (200 masl; 35.58° N, 79.06° W,). A subset of 3 tree cores was then selected for cellulose extraction based on maximum annual ring width. Each tree core was sliced using a microtome into cross-sections approximately 0.5 mm thick. This thickness allowed for multiple observations during early growth years (mean N = 6.5 in 1997), when ring widths were wider, and fewer observations in later years (mean N = 3.0 in 2002) as ring widths diminished. Individual cross-sections were then homogenized and α-cellulose was extracted [*Brendel et al.*, 2000]. Carbon isotopes were measured on the α-cellulose

using a Finnegan MAT Delta Plus XL Isotope Ratio Mass Spectrometer.

2.4. Simulations of the Global Atmospheric CO_2 and $\delta^{13}CO_2$ Budgets

[12] We simulated the global CO_2 budget and its carbon isotopic composition (equation (5)) with total CO_2 and $^{13}CO_2$ treated as independent tracers. The spatial component of fossil fuel fluxes was derived from EDGAR (http://www.mnp.nl/edgar/) and combined with temporal trends from *Marland et al.* [2005]. Due to the limited information on the temporal and spatial variability of isotopic values from different fossil fuel types on a global scale, all fossil fuel fluxes were assigned a $\delta\ ^{13}CO_2$ value of −30.0 ‰. Net fluxes from the terrestrial biosphere were estimated using the steady state "neutral biosphere" from an atmospheric transport model inter-comparison study [*Gurney et al.*, 2002] that was simulated using the Carnegie Ames Stanford Approach (CASA) model, which combines satellite-derived estimates of primary productivity with simulations of terrestrial ecosystem processes [*Randerson et al.*, 1997].

[13] Photosynthetic discrimination, Δ_{al}, was specified according to three different scenarios: i.) a constant 18.0 ‰ globally (Δ18), ii.) a biosphere with entirely C3 vegetation and varying stomatal conductance in response to environmental parameters (ΔC3), iii.) a biosphere with a mixture of C3 and C4 vegetation and varying stomatal conductance in response to environmental variables (ΔC3:C4). Values of Δ_{al} in scenarios ii and iii were calculated according to a multistage transport model of CO_2 that calculates isotopic discrimination from the leaf boundary layer to fixation within the cell [*Suits et al.*, 2005]. The terrestrial isotopic disequilibrium term for gross terrestrial fluxes was estimated using pulse-response functions from CASA by allowing uptake of carbon as net primary productivity (NPP) for one year and then following its monthly release as heterotrophic respiration for 200 years [*Thompson and Randerson*, 1999]. This resulted in an age distribution of heterotrophic respiration for each 1° × 1° land pixel, which was then convolved with the atmospheric $\delta^{13}C$ history [*Francey et al.*, 1999] to give the isotopic signature of the respiratory flux. This approach yielded a global mean carbon residence time of approximately 15 years, which is within the range of previously published values [*Randerson*, 2005], and an NPP-weighted terrestrial isotopic disequilibrium of $\delta_{la} - \delta_{al} \approx 0.33‰$, which is within the range of values reported by *Thompson and Randerson* [1999].

[14] Net ocean fluxes were calculated from ΔpCO_2 estimates and surface wind fields [*Takahashi et al.*, 2002] using the quadratic gas exchange formulation of *Wanninkhof* [1992]. Kinetic isotopic fractionation due to net air-sea gas exchange was taken as the temperature-independent estimate of ε_{ao} = −1.8‰ from *Zhang et al.* [1995]. Oceanic disequilibrium flux was estimated for each ocean pixel by combining surface ocean pCO_2 [*Takahashi et al.*, 2002] and $\delta^{13}C$ measurements of dissolved inorganic carbon from the surface ocean [*Gruber and Keeling*, 2001], while accounting for the equilibrium isotopic fractionation as a function of sea surface temperatures [*Zhang et al.*, 1995]. The global flux-weighted ocean-atmosphere disequilibrium (i.e., $\delta_{oa} - \delta_{ao}$) based on this approach was 0.6‰.

[15] Last, individual fluxes from our global isotopic carbon budget were circulated in the atmosphere using the TM5 chemical transport model [see *Krol et al.*, 2005]. The model was configured at a 6 × 4° grid cell resolution globally and a 1° × 1° grid cell resolution over North America. Transport was driven by European Center for Medium-Range Weather Forecasting meteorological fields. The duration of model simulations was from 2002 to 2006. The transport model took approximately one year to equilibrate and thoroughly mix all tracers in the troposphere; thus, we have excluded 2002 from all analyses. All simulated tracers were then sampled at the same frequency and elevation from the 9 grid cells encompassing our atmospheric sampling sites for comparison with actual atmospheric observations. Seasonal isotopic discrimination was then evaluated by comparing predictions from two independent stomatal conductance models in response to relative humidity data obtained from the North American Regional Reanalysis project (http://www.emc.ncep.noaa.gov/mmb/rreanl/) and vapor pressure deficits calculated from leaf temperatures derived from SiB 2.5 [*Sellers et al.*, 1996].

2.5. Statistical Treatment and Processing of Data

[16] The selection of regression models when fitting the relationship between atmospheric CO_2 and $\delta^{13}C$ is not trivial and the advantages of different regression models have been previously considered [*Miller and Tans*, 2003; *Pataki et al.*, 2003; *Zhou et al.*, 2006]. The consensus is that ordinary least squares regression models that do not include error estimates for the independent x variable (Model I) yield estimates of δ_s that are systematically biased. Alternatively, regression models that include error estimates for both the independent x variable and dependent y variable (Model II) yield more robust estimates of δ_s [*Miller and Tans*, 2003; *Pataki et al.*, 2003]. For this analysis we selected the FITEXY function [*Press et al.*, 1992] from a family of Model II type regression models because of its flexibility and proven effectiveness [*Miller and Tans*, 2003]. All observational data were filtered to remove anomalous values exceeding 3 σ that may contribute disproportionately to our regression models. Because our analysis is focused on the seasonal cycle of CO_2 and $\delta^{13}CO_2$, long-term trends in simulated data were removed. For this analysis we considered two classes of background atmospheric reference curves: i.) those that are generated from the intrinsic variability of the data at any given site and ii.) those that are generated from independent observational data. For the generation of background reference curves based on the intrinsic variability in both observed and simulated CO_2 and $\delta^{13}CO_2$ data, we constructed curves of the long-term trend and seasonal cycle according to *Thoning et al.* [1989]. The long-term trend curve was fit using a polynomial with 3 terms and a low-pass filter with full-width at half-maximum (FWHM) of 390 days, whereas the seasonal cycle curve was fit with 4 harmonic terms and a low-pass filter of FWHM of 30 days (see *Thoning et al.* [1989] for details). Independent background reference curves for CO_2 and $\delta^{13}CO_2$ were derived for the marine boundary

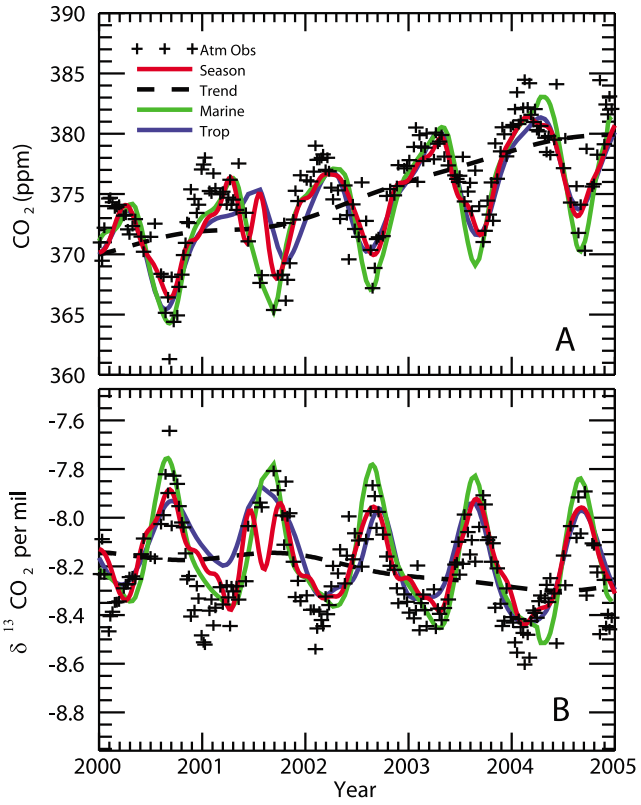

Figure 1. Atmospheric observations of CO_2 and $\delta^{13}CO_2$ from UTA compared with different background reference curves from 2000 to 2005. (a) Concentration of atmospheric CO_2 and (b) its carbon isotopic signature ($\delta^{13}CO_2$ ‰). Superimposed on the observed data (Atm Obs, +) are the seasonal cycle (Season; red), the smooth trend (Trend; black dashed), the marine boundary layer (Marine; green) and the free troposphere (Trop; blue). The seasonal cycle and the smooth trend were calculated over an evenly spaced weekly interval from the observed time series (see *Thoning et al.* [1989] for details). The marine boundary layer curve was constructed from an aggregate of observations from marine sites at comparable latitudes (35 °N to 45 °N) and for our free troposphere background curve we used data from Niwot Ridge, Colorado (3475 masl; 40.05° N, 105.58° W). Similar plots showing the range of background reference curves for LEF (Figure S1) and ITN (Figure S2) can be found in the auxiliary material.

layer and the free troposphere. The marine boundary layer curve was generated based on a composite of marine sites found at similar latitudes [*Masarie and Tans*, 1995] and the free troposphere curve was generated from measurements at Niwot Ridge, CO (see Section 2.2 above).

[17] Because the exact date of cellulose synthesis was unknown, we assumed that isotopic measurements were distributed evenly over the growth season and correspond to monthly values ±1 month [*Moore et al.*, 2006]. Thus, we derived a 3 month moving window approach for estimating δ_s for comparison with the tree ring isotope data. Based on this approach the previous month and the following month were included when calculating δ_s for the current month. For example, in estimating δ_s for January we also included December and February (DJF) and for estimating δ_s for February we included JFM. This approach yielded a smoother representation of the seasonal cycle that better resembled the smooth spline fit to the seasonal isotopic tree ring data.

3. Results and Discussion

3.1. Observations of Seasonal Isotopic Cycles in the Atmosphere

[18] The selection of a background reference curve is not trivial, and different background references may provide information about processes at different spatial scales. Perhaps the background reference curve with the fewest assumptions, that may integrate processes over the widest geographic extent, is the long-term trend in atmospheric CO_2 derived from a time series of the actual data. By subtracting this smooth representation of the increase in CO_2 (Figure 1a) or the decrease in $\delta^{13}CO_2$ (Figure 1b), the maximum variance in residuals is retained (i.e., the seasonality of the data). An alternative reference curve for specifying the background concentration of atmospheric CO_2 is by subtracting the smoothed seasonal fit to the actual data [*Bakwin et al.*, 1998]. Although this curve more closely captures the full range of seasonal variability in the data (Figure 1), fitting this curve to the data requires more parameters and thus more assumptions. By subtracting the seasonal background curve from the data, the residual variance due to low frequency global or hemispheric processes is minimized, whereas the high frequency variability due to local or regional processes is maximized. Instead of deriving a reference curve from the observed variability in the data, it may be desirable to use independent data in specifying background concentrations. One such approach is to subtract marine boundary layer values at the same latitude from the observed concentrations at a continental site (Figure 1). Such an approach may be useful for comparing the uptake or release of carbon by the terrestrial biosphere. Finally, a background reference curve may be generated from the free troposphere above the site to identify sources and sinks affecting boundary layer CO_2 and $\delta^{13}CO_2$ at a regional scale (Figure 1) [*Bakwin et al.*, 2004; *Helliker et al.*, 2004].

[19] Atmospheric observations coincide more closely with background values during certain periods of the year. At UTA atmospheric CO_2 observations tend to exceed all background values during winter months (Figure 1a), and $\delta^{13}CO_2$ tends to be more depleted than background values during winter months (Figure 1b). At LEF a similar trend is evident with observed atmospheric CO_2 concentrations exceeding those of all the background reference curves during the winter months (Figure S1a), but with observed $\delta^{13}CO_2$ values mainly exceeding background values during summer months (Figure S1b).[1] Last, background reference curves at ITN tend to fall below observed atmospheric CO_2 concentra-

[1]Auxiliary materials are available with the HTML. doi:10.1029/2009GB003623.

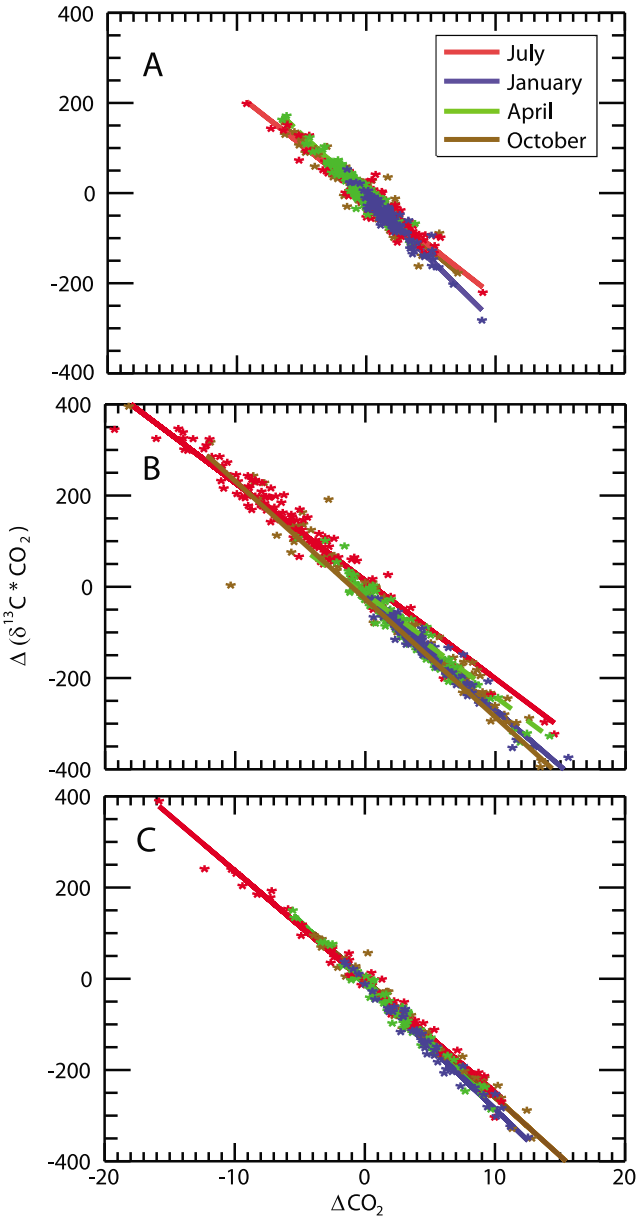

Figure 2. Residual differences in atmospheric CO_2 and $\delta^{13}C$. The x axis in each panel represents CO_2 anomalies with respect to the background free troposphere and each y axis represents anomalies in the product of CO_2 and $\delta^{13}C$ with respect to the background free troposphere. Changes in slopes are indicative of changes in the isotopic signature of source CO_2 (δ_s) for January, April, July, and October for three different atmospheric sampling stations (a) UTA, (b) LEF, and (c) ITN.

tions (Figure S2a) and exceed $\delta^{13}CO_2$ values mainly during the winter months. In some instances peaks in observations are out of phase with background reference peaks. At all sites and in most years during winter months observed CO_2 levels tend to lead maxima in CO_2 of the marine boundary layer and free troposphere (Figures 1a, S1a, and S2a). This winter lag is also evident between $\delta^{13}CO_2$ observations and the marine boundary layer as well as the free troposphere (Figures 1b, S2b, and S3b). However, all background reference curves appear to be more in phase with observations during summer minima in atmospheric CO_2 and maxima in $\delta^{13}CO_2$.

[20] Once the background reference curve has been subtracted from the atmospheric observations, the residual anomalies of CO_2 and the product of $\delta^{13}CO_2$ and CO_2 can be plotted to solve for the slope (i.e., δ_s). Here we calculate differences between observations and the background curve from the free troposphere at a monthly time step to identify seasonal changes in δ_s (Figure 2). Based on this approach, we see that positive anomalies in CO_2 are observed during winter months and negative anomalies in CO_2 are observed during summer months (albeit with greater variability). Across all sites δ_s values are negative throughout the year; however, significant changes in slope occur coherently among all sites (Figure 2). The slopes become less negative in July, indicating isotopic enrichment of δ_s, and more negative in January, indicating isotopic depletion of δ_s, with intermediate slopes in the fall and spring (Figure 2).

[21] If we plot the δ_s values for each month of the year, we see that the apparent seasonal cycle in δ_s is coherent across our three sampling sites and persistent, regardless of residual technique selected (Figure 3). This is evidenced by the peak-to-trough amplitude of the seasonal cycle in δ_s (4–6‰), which greatly exceeds error estimates for any given month (approximately 2‰). The greatest amplitude in seasonal cycle is at UTA where winter values of δ_s are much more depleted (~−30‰) than summer values (~−24‰) with values peaking between July and September (Figure 3a). There is no apparent difference between residual techniques used to infer δ_s at UTA, as all δ_s values are bound by the error estimates. Although there does appear to be a seasonal cycle in δ_s at LEF of approximately 4‰, it is greatly dampened (Figure 3b). Residuals calculated from the troposphere and the long-term trend show a consistent peak in δ_s values in July and August, whereas residuals calculated from the seasonal cycle show only a slight enrichment during summer months and residuals calculated from the marine boundary layer show no pronounced seasonal peak (Figure 3b). Last, a prominent seasonal cycle of ~4‰ is apparent at ITN as well, where δ_s values peak in August (Figure 3c). All the residual techniques at ITN yield a similar seasonal pattern, except for the seasonal cycle that has an anomalous peak in June. Although there are slight differences between these North American sites in the amplitude and phasing of the seasonal cycle in δ_s, the seasonal cycle with more enriched δ_s values during summer months is unequivocal. Furthermore, the seasonal cycle is persistent regardless of residual technique selected, suggesting that it is in fact a robust feature of the atmosphere over North America and not an artifact of our analytical approach. This coherent seasonal cycle in δ_s suggests either a temporal change in the relative fluxes from the land, ocean, or fossil fuels, or else a change in the isotopic composition of these fluxes.

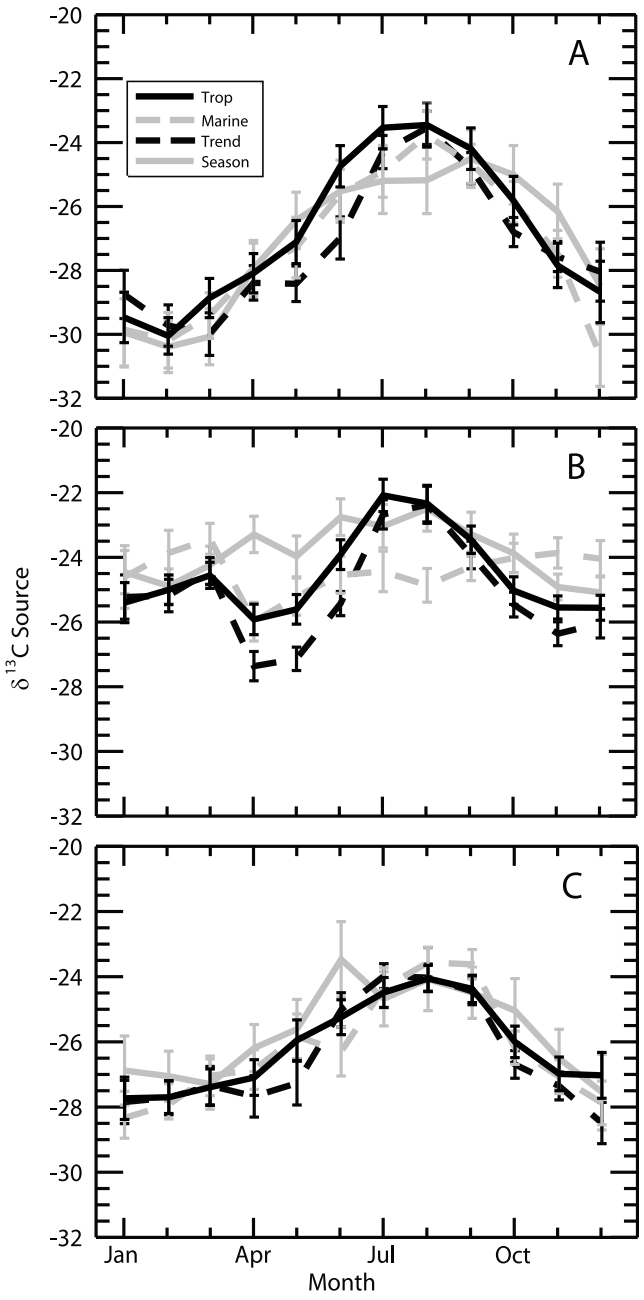

Figure 3. The apparent seasonal cycle in isotopic composition of source CO_2 (δ_s) to the atmosphere. Plotted are the slopes from the residual analyses (see Figure 2) based on 4 different background reference curves: (1) residuals from the long-term trend (black dashed), (2) residuals from the free troposphere (black solid), (3) residuals from the marine boundary layer (gray dashed), and (4) residuals from the seasonal cycle (gray solid). Monthly values from the entire time series (1993–2006) have been combined to produce a seasonal climatology. Error bars represent the standard error of the slope fit to data from each month. Data are plotted for (a) UTA, (b) LEF, and (c) ITN.

3.2. Simulations of Seasonal Isotopic Cycles in the Atmosphere

[22] Our global simulations perform remarkably well at capturing seasonal variability in both CO_2 and $\delta^{13}CO_2$ concentrations in the atmosphere (Figure 4). The amplitude of the annual cycle of approximately 15 ppm CO_2 and 0.7‰ $\delta^{13}CO_2$ observed at UTA is captured by our simulations. According to model simulations this annual cycle is primarily due to seasonal variability in the net land fluxes and to a lesser extent pulses of fossil fuel emissions trapped in the boundary layer during winter months and released during summer months (Figure 4a). Similar seasonal patterns dominated by terrestrial processes are observed at LEF (Figure S3). Although ocean fluxes are a significant contribution to the global carbon budget, there is no apparent seasonal cycle in net ocean fluxes at our continental sites (Figures 4 and S3). Atmospheric values of $\delta^{13}CO_2$ largely mirror CO_2 values and are dominated by terrestrial photosynthesis and respiration (Figure 4b). Thus we may conclude that this model does an excellent job simulating the seasonal cycles in CO_2 and $\delta^{13}CO_2$.

[23] We sampled the model atmosphere to determine how effective our residual techniques (i.e., equation (3)) are at capturing the seasonal cycle of photosynthetic discrimination, and which background reference is the most reliable proxy for C_{bg} and δ_{bg}. First, we compare our null model (Δ_{al} = 18 ‰) to δ_s inferred from the total atmosphere (including all terms in equation (5)) and we see that all residual techniques underestimate δ_s for most of the year, except during summer months (Figures 5a, 5d, and 5g). However, using the free troposphere as the back ground concentration, results in the least amount of residual seasonal variability. The δ_s derived from our residual techniques during winter months are probably biased low due to fossil fuel emissions, which have been assigned an isotopic signature of −30‰. This was confirmed by removing the fossil fuel term ($\delta_f F_f$) from our global budget (equation (5)) and re-calculating δ_s yielding a mean of 25.99 ‰ (Figure S4a), with very little seasonal variability (sd = 0.3 ‰). Last, we used our null model to examine only fluxes from the terrestrial biosphere, where all terms in equation (5) not containing N_l are set to zero. Under these conditions, all of our residual analysis techniques do well at retrieving the terrestrial signal of approximately −26‰ (i.e., −8 ‰ + −18‰), indicating that our residual approach is effective for inferring isotopic discrimination from the terrestrial biosphere (Figure S4b). However, seasonal biases due to changes in F_f or δ_f of fossil fuels are unavoidable when sampling the actual atmosphere, especially during winter months. Thus taking the difference with respect to the free troposphere is the most effective technique for inferring δ_{al} of the biosphere due to its low seasonal variability based on our simulations.

[24] If we consider the scenario of strictly C3 vegetation we see considerable variability in δ_s between sites (Figure 5 and Table 1). At UTA we see a strong seasonal cycle in the atmosphere with isotopic enrichment peaking in June that closely parallels the isotopic signature of the biosphere (δ_{al}) even when fossil fuels are removed from the budget

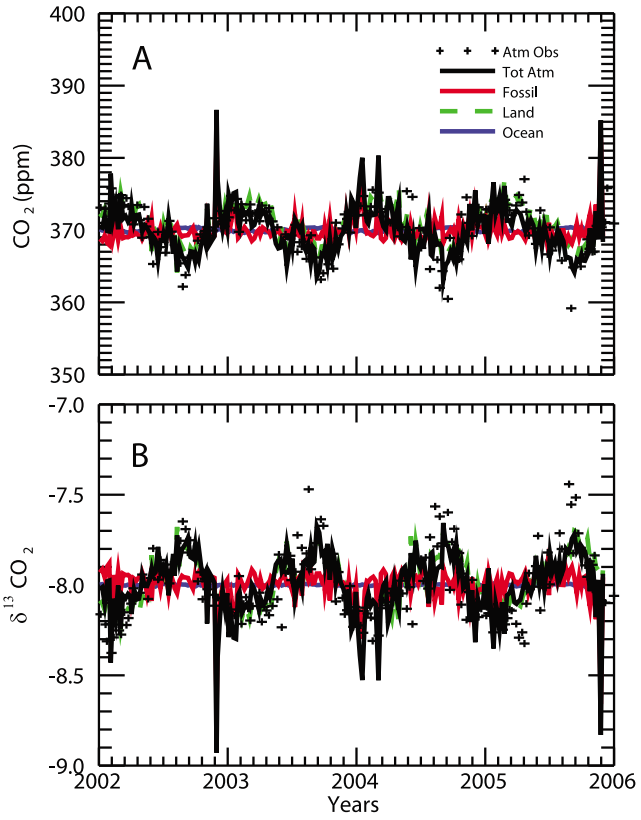

Figure 4. Model simulations of the detrended seasonal cycle of different components of the global carbon cycle compared to atmospheric observations at UTA. Superimposed on the atmospheric observations (+) are the total atmospheric concentration of (a) CO_2 and (b) its carbon isotopic signature ($\delta^{13}CO_2$) plotted as solid black lines. Fossil fuel emissions and their isotopic signature are plotted as red lines. Net fluxes from the land are plotted as a dashed green line and net fluxes from the ocean are plotted as a blue line. Isotopic disequilibria for gross land and ocean fluxes have no apparent seasonal cycle and thus are not included in these plots. All tracers were simulated using the coupled biosphere-transport model with the mixed ΔC3:C4 vegetation scenario. A similar correspondence was found between atmospheric observations and model simulations for LEF (Figure S3). Observations and simulations of the raw data from ITN were not reported because of their lack of temporal correspondence.

(Figure 5b). Model simulations with only a C3 biosphere agree fairly well with observations at UTA (RMSE = 2.36). In contrast, at LEF we see a relatively flat seasonal cycle in both the atmosphere and δ_{al} even when fossil fuels are removed from the budget (Figure 5e). Although there is little seasonal variability in δ_s at LEF, ΔC3 model simulations are fairly close to atmospheric observations (RMSE = 2.05). There is also a summer peak evident in our ΔC3 simulations of δ_s at ITN (Figure 5h) that closely corresponds to the seasonal cycle observed at ITN (RMSE = 0.89).

[25] In conclusion, if we consider the mixed C3:C4 vegetation scenario (i.e., ΔC3C4), which most closely resembles the actual biosphere, we see that the entire atmosphere has shifted toward more enriched values due to decreased discrimination by C4 photosynthesis (Figure 5). Although the distinct peak in enrichment of δ_s is still evident in the total atmosphere at UTA more enriched values during winter months make the annual cycle less prominent (Figure 5c). Despite the apparent dampening of the seasonal cycle by C4 vegetation at UTA, the model more closely captures atmospheric observations (RMSE = 1.97). The inclusion of C4 vegetation at LEF has actually resulted in more of an annual cycle in δ_s, with more enriched values in the winter months and more depleted values in the summer (Figure 5f), that more closely resembles atmospheric observations (RMSE = 1.84). Similarly, more enriched winter values of δ_s have greatly dampened the seasonal cycle at ITN (Figure 5l). Although the summer peak is still evident at ITN under the ΔC3C4 scenario, the inclusion of C4 vegetation at this site actually reduces the correspondence between observations and simulations (RMSE = 1.38). Generally, the removal of fossil fuels from the atmospheric budget resulted in more enriched values of δ_s that corresponded better with δ_{al} at all three sites (Figure 5).

[26] Therefore, based on our model simulations, the most effective residual technique for retrieving information on terrestrial fluxes from observations in the planetary boundary layer is by specifying background concentrations of CO_2 and $\delta^{13}CO_2$ from the free troposphere. This residual technique is most effective for inferring isotopic discrimination of the terrestrial biosphere during summer months and when comparing data from multiple sites on a regional to global scale. Although seasonality in δ_s can be attributed to seasonality in Δ_{al} for much of the year, our model analysis suggests that fossil fuel emissions and ocean fluxes can also influence the seasonal distribution of δ_s. One persistent problem with this approach is discerning between respiratory and fossil fluxes, especially during the winter months. Attempts to further isolate the Δ_{al} signal from the biosphere by using CO/CO_2 emission ratios at ITN [*Bakwin et al.*, 1998] were only slightly helpful in removing local fossil fuel emissions from the seasonal cycle. A novel approach of measuring anomalies in mass 47 CO_2 (primarily composed of $^{13}C^{18}O^{16}O$) has been developed to distinguish between CO_2 evolved from low-temperature respiration and high temperature combustion; however, it is uncertain whether this approach will be able to resolve seasonal differences in these fluxes [*Affek et al.*, 2007]. Our analysis suggests that measurements of atmospheric CO_2 and $\delta^{13}CO_2$ made at NWR are representative of the free troposphere over North America. Observations at NWR have already been used as a background reference in previous studies of ^{14}C to quantify locally derived [*Turnbull et al.*, 2006] and regionally derived fossil fuel emissions [*Hsueh et al.*, 2007] and our analysis verifies that NWR is probably the best background reference for North America. Comparisons between models and observations indicate that the source of CO_2 to the

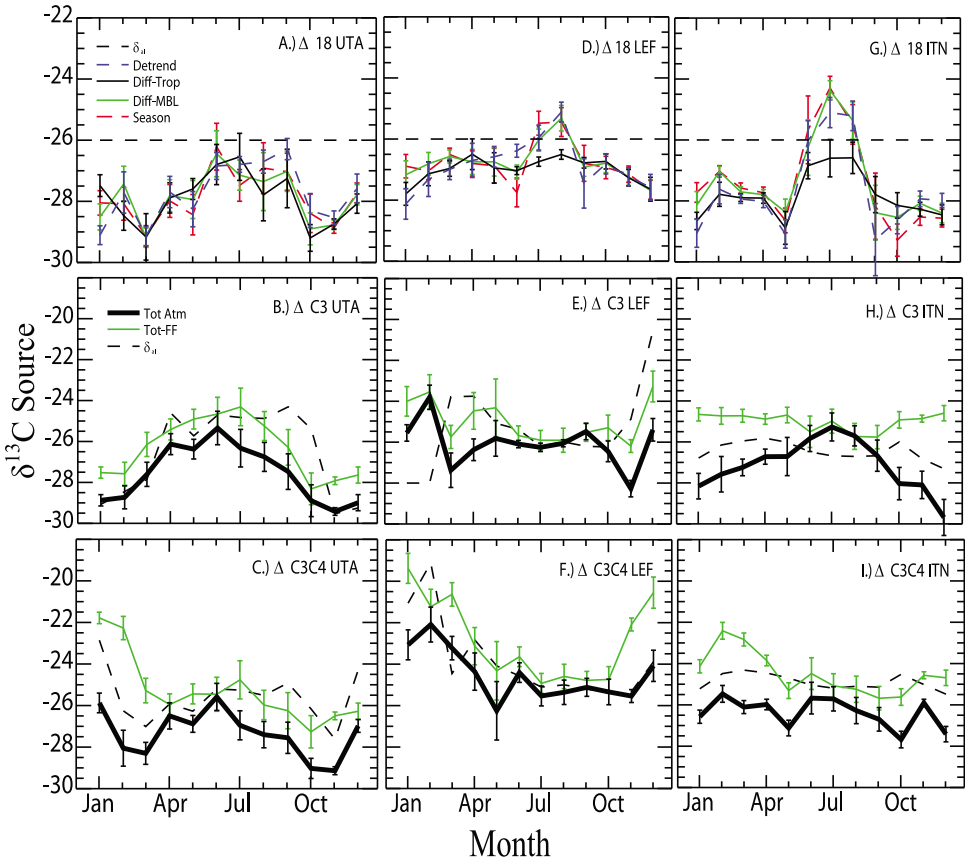

Figure 5. Model simulations of the isotopic signature of source CO_2 (δ_s) at (a, b, and c) UTA, (d, e, and f) LEF, and (g, h, and i) ITN. Monthly values of δ_s are plotted for the three different discrimination scenarios: constant Δ_{al} = 18 ‰ (Figures 5a, 5d, and 5g), Δ_{al} as a function of just C3 vegetation Figures 5b, 5e, and 5h), and Δ_{al} as a function of mixed C3:C4 vegetation (Figures 5c, 5f, and 5i). The four different residual techniques are compared with δ_{al} (dashed black line) under constant discrimination (Figures 5a, 5d, and 5g). Simulated values of varying isotopic discrimination compared to δ_{al} based on the residuals calculated from the free troposphere where the Tot Atm equals the total atmosphere and Tot-FF equals the total atmosphere minus fossil fuels.

atmosphere can be inferred from atmospheric measurements; however, it is difficult to distinguish which fluxes are driving the apparent seasonal cycle of δ_s without independent information.

3.3. Observations and Simulations of Seasonal Isotopic Cycles in the Biosphere

[27] We can use independent observations from the biosphere to verify the extent to which terrestrial processes are influencing the isotopic variability of CO_2 in the atmosphere. Our intra-annual tree ring measurements show a clear increase in $\delta^{13}C$ over the course of the growing season (Figure 6a). Values of $\delta^{13}C$ range from −28.7‰ to −24.8‰ with a mean of −26.8‰ and most trees showing an increase in $\delta^{13}C$ of about 1 to 2‰ during the summer growth season (Figure 6a). Although some of this seasonal variability in cellulose $\delta^{13}C$ can be attributed to changes in atmospheric $\delta^{13}CO_2$ used as a substrate during photosynthesis, the observed change in atmospheric $\delta^{13}CO_2$ during the growth season at ITN is on the order of 0.2‰, which is not enough to explain the range in observed cellulose $\delta^{13}C$ values. These intraannual measurements of $\delta^{13}C$ in the cellulose of trees can be compared directly with isotopic predictions from the SiB 2.5 biosphere model (i.e., δ_{al}). In contrast to our observations of $\delta^{13}C$ in trees, model simulations of δ_{al} show a clear decrease of approximately 1‰ during the growth season indicative of increased isotopic discrimination by the terrestrial biosphere (Figure 6a). Thus observations and simulations of $\delta^{13}C$ in the terrestrial

Table 1. Root Mean Squared Error Estimates for δ_s Values Calculated From Atmospheric Observations and Model Simulations[a]

Sampling Site	Δ18	ΔC3	ΔC3C4
UTA	2.17	2.36	1.97
LEF	2.73	2.05	1.84
ITN	1.91	0.89	1.38

[a]RMSE values are reported in units of ‰ for our 3 sampling sites and our 3 model scenarios. Optimal model fits are indicated by reduced RMSE values.

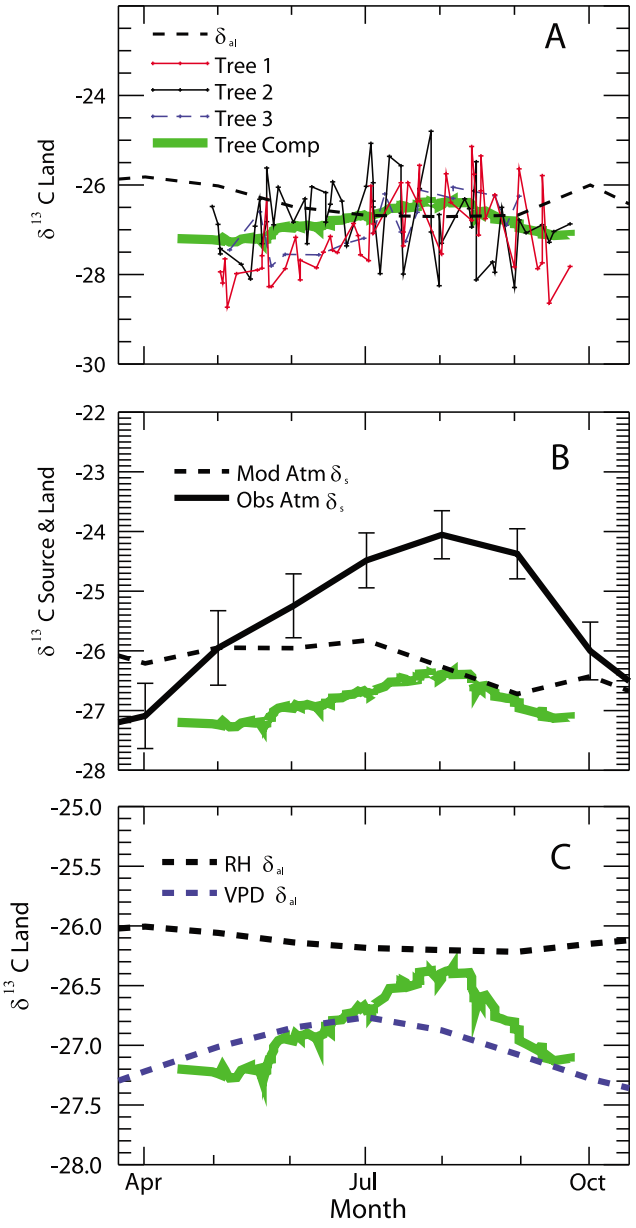

Figure 6. Comparison of seasonal variability in $\delta^{13}C$ of land and sources of CO_2 to the atmosphere from observations and model simulations.(a) Measurements of $\delta^{13}C$ in cellulose of trees growing in Duke Forest compared with $\delta^{13}C$ of the land due to fractionation by C3 vegetation in our biosphere model (δ_{al}). Data points indicate individual $\delta^{13}C$ measurements from growth years spanning 1997 to 2002. Spline functions were fit to data to approximate seasonal distributions of $\delta^{13}C$ for different trees and a composite of all observations from all years (Tree comp; green line). (b) Observed $\delta^{13}C$ source (δ_s) values from the atmosphere derived from tropospheric residuals at ITN (solid line) compared with simulated values of δ_s and our tree ring composite. (c) Estimates of δ_{al} from our revised stomatal conductance models where conductance varies as a function of relative humidity (RH) or vapor pressure deficit (VPD) compared with our tree ring composite.

biosphere both show apparent seasonal cycles, but these seasonal cycles are clearly out of phase.

[28] A consistent increase in δ_s during the growth season is also inferred from our atmospheric measurements (Figure 6b). The amplitude in the seasonal cycle of δ_s inferred from residual differences from the free-troposphere at this site is approximately 3‰ with maximum values occurring in August. Although atmospheric observations of δ_s at ITN are fairly consistent with model predictions of δ_s during spring months, the two clearly diverge from July through September (Figure 6b). This divergence is primarily due to increased discrimination by the modeled terrestrial biosphere (Figure 6a), which accounts for most of the CO_2 flux during summer months.

[29] The pronounced seasonal cycle of δ_s inferred from atmospheric observations appears to be in phase with the seasonal cycle of $\delta^{13}C$ observed in trees growing nearby (Figure 6b), but with two key differences. The amplitude in the seasonal cycle of δ_s inferred from the atmosphere (~3‰) is greater than the amplitude of the seasonal composite of $\delta^{13}C$ in our trees (1–2‰). This apparent attenuation of the seasonal cycle in the biosphere may be an artifact of combining observations of $\delta^{13}C$ from cellulose with no precise date of formation from three different trees and multiple years. Although you would expect this approach to lead to a very smooth representation of the seasonal cycle in the biosphere, you would expect the seasonal cycle in the atmosphere to be fairly smooth as well because the atmosphere is integrating across many types of vegetation over many years. The second difference is the observed isotopic offset between cellulose $\delta^{13}C$ (mean ≈ −27‰) and δ_s inferred from the atmosphere (mean ≈ −25.5‰) during the summer months (Figure 6c). Based on our analysis, fossil fuels tend to deplete the atmosphere (Figure 5); thus, it is possible that a fossil fuel source could be causing a slight depletion in the seasonal isotopic cycle observed in our trees which would account for the slight offset from the atmosphere. Another possible explanation for these slightly depleted $\delta^{13}C$ values is the recycling of respired air which would be relatively depleted compared to the atmosphere at this site [*Keeling*, 1961]. Therefore the relatively depleted values of $\delta^{13}C$ observed in our trees compared to δ_s inferred from the atmosphere are most likely due to a depleted source of CO_2 (e.g., fossil fuels or respired CO_2) serving as a substrate during photosynthesis. This provides evidence that the isotopic signature imparted to the atmosphere by the biosphere can be inferred from atmospheric measurements, especially during summer months, but that fossil fuel emissions and ocean fluxes may confound the isotopic signature of the biosphere during certain months.

[30] The observed seasonality in $\delta^{13}C$ of cellulose in trees is not unique to trees growing in the Southeastern USA. Similar seasonal patterns of cellulose $\delta^{13}C$ have been observed in a range of tree species growing in Southwestern USA [*Leavitt et al.*, 2002] in Southern France [*Ogée et al.*, 2009], New Zealand [*Barbour et al.*, 2002], and the tropics of Thailand [*Poussart et al.*, 2004]. These coherent seasonal patterns of $\delta^{13}C$ observed in trees globally are suggestive of a common physical mechanism driving isotopic discrimination by the biosphere and because of the large

terrestrial gross return flux to the atmosphere are suggestive of a large isotopic imprint on the atmosphere by the biosphere. In fact, the enriched values of cellulose $\delta^{13}C$ during January and February of trees growing in the Southern Hemisphere [*Barbour et al.*, 2002] are perfectly out of phase with the seasonal pattern of cellulose $\delta^{13}C$ in trees growing in the Northern Hemisphere, suggesting that the seasonal cycle of δ_s in the overlying atmosphere of the Southern Hemisphere should be out of phase with the Northern Hemisphere as well. This prediction can be tested directly by analyzing atmospheric observations of CO_2 and $\delta^{13}CO_2$ in the Southern Hemisphere in the same manner as we have described in this study.

[31] Measurements of $\delta^{13}C$ in the biosphere and δ_s inferred from the atmosphere indicate a progressive isotopic enrichment of the biosphere during the growth season due to a decrease in Δ_{al}; however, this is completely opposite to the isotopic composition of leaf wax esters that indicate an increase in Δ_{al} during the Northern Hemisphere summer [*Conte and Weber*, 2002]. One possible explanation for why Δ_{al} inferred from these different methods is out of phase is that cellulose could have been synthesized from different carbohydrate pools and thus reflects the different isotopic signatures from these various carbohydrate pools. However, recent model simulations of cellulose in tree rings of *Pinus pinaster* have determined that much of the seasonal variability in both carbon and oxygen isotopes can be explained from a single carbohydrate pool [*Ogée et al.*, 2009]. Furthermore, growth studies of *Pinus taeda* using isotopically labeled CO_2 suggest that cellulose is synthesized from atmospherically fixed carbon within weeks to months (A. P. Ballantyne unpublished data, 2002). An alternative explanation for the phase discrepancy between Δ_{al} inferred from these different methods is that leaf wax esters collected in Bermuda (32° N 64° W) may have been transported from source regions other than North America. In a follow up study, *Conte et al.* [2003] have demonstrated that the isotopic composition of leaf wax esters is in fact representative of the biosphere with values 6‰ depleted in ^{13}C relative to plant carbon at a prairie site in North America; however, they were unable to document any clear seasonal cycle in the isotopic composition of leaf wax esters. Thus further research into the physiological mechanisms controlling the isotopic composition of cellulose and leaf wax esters is necessary before these apparent seasonal cycles in isotopic discrimination can be extrapolated to global scales.

[32] We have presented two independent lines of evidence suggesting that the amount of isotopic discrimination (i.e., Δ_{al}) by the terrestrial biosphere in central North Carolina decreases during the growth season: i.) intraannual measurements of $\delta^{13}C$ in the cellulose of trees show an increase during the growth season and ii.) monthly values of δ_s inferred from the atmosphere also show an increase during the growth season. However, these observations are at odds with model simulations indicating an increase in Δ_{al} of the biosphere during the growth season. This discrepancy suggests that these pine trees growing in North Carolina may not be representative of the local biosphere, or that another mechanism besides isotopic discrimination by the biosphere is driving seasonal variability in δ_s inferred from atmospheric measurements. An alternative explanation, as we suggest below, is that another physical mechanism may be driving stomatal conductance and ultimately changes in Δ_{al}.

4. Revised Conductance Model Accounts for Isotopic Discrimination by the Biosphere

[33] The amount of carbon assimilated (A) and water transpired (E) during photosynthesis by the biosphere is largely determined by stomatal conductance. The relationship between E (mol m^{-2} s^{-1}) and conductance of H_2O (g_w; mol m^{-2} s^{-1}) from stomata is often described by the following relationship [*Farquhar and Sharkey*, 1982]:

$$E = g_w(w_i - w_a), \tag{9}$$

where w_i and w_a represent the molar fractions (mol mol^{-1}) of saturated water inside the leaf and in the atmosphere, respectively. A similar equation describing the relationship between assimilation (A; mol m^{-2} s^{-1}) and conductance of CO_2 (g_c; mol m^{-2} s^{-1}) can be written following *Farquhar and Sharkey* [1982]:

$$A = g_c(c_a - c_i). \tag{10}$$

where c_a and c_i represent the concentrations of CO_2 in the atmosphere and in the leaf (mol mol^{-1}). The quantity $(c_a - c_i)$ on the right hand side of equation (10) can then be expressed as $c_a(1 - {}^{c_i}/_{c_a})$ to demonstrate that ${}^{c_i}/_{c_a}$ is a sensitive indicator of stomatal conductance.

[34] Stomatal conductance is the primary factor affecting the variability of isotopic discrimination (i.e., Δ_{al}) during photosynthesis. Discrimination against the heavier isotope of carbon dioxide ($^{13}CO_2$) by C3 vegetation in the terrestrial biosphere can then be approximated, neglecting respiration, as the fractionation during diffusion (a = 4.4‰) and carboxylation by Rubisco (b = 27‰) [*Farquhar et al.*, 1989], such that:

$$\Delta_{al} = a + (b - a){}^{c_i}/_{c_a} \tag{11}$$

Therefore according to equation (10), if A remains constant, an increase in stomatal conductance must be accompanied by enhanced ${}^{c_i}/_{c_a}$ and ultimately increased isotopic discrimination due to carboxylation (equation (11)).

[35] Several empirical models of stomatal conductance have also been derived from leaf level measurements of gas exchange [see *Katul et al.*, 2000]. Because conductance of H_2O and CO_2 occurs simultaneously through stomates, the independent formulas for conductance (equations (9) and (10)) are conventionally combined into a single equation in terms of g_c. In SiB 2.5, g_c is formulated according to the widely used Ball-Berry relationship [*Ball*, 1988], whereby:

$$g_c = m\frac{(AR)}{c_a} + b. \tag{12}$$

According to this relationship, stomatal conductance is enhanced by increased relative humidity at the leaf surface (R) and diminished by increased atmospheric CO_2 (c_a), where m and b represent empirical constants that vary

according to vegetation type [*DeWar*, 2002; *Katul et al.*, 2000].

[36] Such an increase in g_c should result in increased discrimination and ultimately more negative values of δ_{al} during the growth season at ITN, which is in fact what is seen for the land surface of central North Carolina in our SiB simulations (Figure 6a). However, this is not what is directly observed in the tree rings, nor indirectly inferred from the atmosphere.

[37] More recent studies have suggested that the physical force driving g_c is actually the vapor pressure deficit (D), which is equivalent to the difference between saturation vapor pressure (e_s) and actual vapor pressure (e_a) [*Katul et al.*, 2000; *Leuning*, 1995]. The dependence of stomatal conductance on D has been expanded by *Leuning* [1995] to include additional empirical terms, such that

$$g_c = g_o + m_L \frac{A}{(c_a - \Gamma)\left(1 + \frac{D}{D_o}\right)}, \tag{13}$$

where g_o is the stomatal conductance at the light compensation point and Γ is the CO_2 compensation point, which varies as a function of temperature. Last, m_L and D_o are empirical coefficients (see *DeWar* [2002] for details). It is apparent from equation (13) that an increase in D will result in decreasing g_c, ultimately leading to diminished discrimination and higher values of δ_s. In order to solve for isotopic discrimination a series of closure models have been proposed [*Katul et al.*, 2000], whereby the expression for assimilation (equation (10)) is substituted into the numerator for A in both stomatal conductance models (equations (12) and (13)). Thus, if we neglect the constant b [*Baldocchi and Harley*, 1995] in the original Ball-Berry model (equation (12)) and substitute in the formula for A (equation (10)) we get the following expression:

$$c_i/c_a = 1 - \frac{1}{mR}. \tag{14}$$

This allows us to solve for isotopic discrimination as a function or relative humidity without knowledge of assimilation. To solve this expression we used a value of $m = 6.0$ that has been empirically fit to *Pinus taeda* growing at this site [*Katul et al.*, 2000] and mean monthly values of relative humidity obtained from North American Regional Reanalysis (NARR) database for the four grid cells surrounding our study site. A similar expression can be derived for the Leuning model of conductance, such that:

$$c_i/c_a = 1 - \frac{1 - \frac{\Gamma}{c_a}}{m_L}\left(1 + \frac{D}{D_o}\right). \tag{15}$$

This expression can then be solved as a function of changing leaf temperature and vapor pressure deficit. Mean monthly values of relative humidity and leaf temperature for the four 32km × 32km degree NARR grid cells surrounding our study site were used to estimate values of Γ and D. Values for the empirical parameters $m_L = 4.0$ and $D_o = 3.0$ were fit using gas exchange measurements at the site [*Katul et al.*, 2000]. Because cellulose tends to be enriched relative to photosynthate, a constant enrichment value of 2 ‰ [*Gleixner et al.*, 1993] was added to our estimates of δ_{al} for comparison with $\delta^{13}C$ values measured in cellulose from the biosphere.

[38] We would expect similar seasonal predictions of stomatal conductance from both models in environments where relative humidity and vapor pressure deficit are negatively correlated and differing predictions in environments where relative humidity and vapor pressure deficit are positively correlated. In arid environments, such as UTA where R and D are inversely related (Figures S5b and S5f), these two formulations of stomatal conductance (equations (14) and (15)) yield similar seasonal patterns of δ_{al} (Figure S6b). However, in the Southeastern, U.S. where the growing season is both hot and humid, R and D increase proportionally (Figure 7). During winter months in central North Carolina, typical values of e_a (≈0.7 KPa) and e_s (≈0.9 KPa) result in low vapor pressure deficits ($D \approx 0.2$ KPa) as well as reduced relative humidity ($R \approx 77\%$). In contrast, during summer vapor pressure values increase by a factor of four e_a (≈3.0 KPa) and e_s (≈3.5 KPa) resulting in increases in both vapor pressure deficit ($D = 0.5$ KPa) and relative humidity ($R = 86\%$) (Figures 7a and 7c). The positive temporal covariance in D and R at this location leads to opposing isotopic effects depending on which conductance model is selected. The original Ball-Berry model predicts an increase in stomatal conductance resulting in increased Δ_{al} and ultimately decreased values of δ_{al} during summer months (Figure 6c). In contrast, the Leuning model predicts a relative decrease in stomatal conductance resulting in decreased Δ_{al} values and ultimately increasing values of δ_{al} during summer months (Figure 6c). Although isotopic predictions from the Leuning model are generally consistent with isotopic observations from the biosphere and the atmosphere, there is a slight lag between the predictions (Figure 6) based on D (peaking in July) and isotopic measurements in tree rings and δ_s values inferred from the atmosphere (peaking in August). Predictions from these two stomatal conductance models are somewhat equivocal for LEF in Wisconsin where D and R are not nearly as temporally covariant (Figures S5a and S5e) and stomatal conductance seems to be responsive to decreases in R in the spring and increases in D in the summer (Figure S6a). These results suggest that different stomatal conductance models may yield very different estimates of carbon and water exchange between the biosphere and atmosphere under certain climatic regimes.

[39] Although models of stomatal conductance are based on physical processes, the physiological mechanisms controlling conductance remain poorly understood. Thus, the models are empirically derived from observations of certain plant species growing under controlled environmental conditions. Therefore it cannot be expected that any one stomatal conductance model can be applied globally to different biomes under a wide range of climatic regimes. However, our results identify specific climatic conditions under which two commonly used stomatal conductance models [*Ball*, 1988; *Leuning*, 1995] yield very different seasonal patterns of isotopic discrimination and thus conductance of CO_2 and H_2O. The discrepancy between these models arises when vapor pressure deficit (i.e., D) and relative humidity (i.e., R), the two

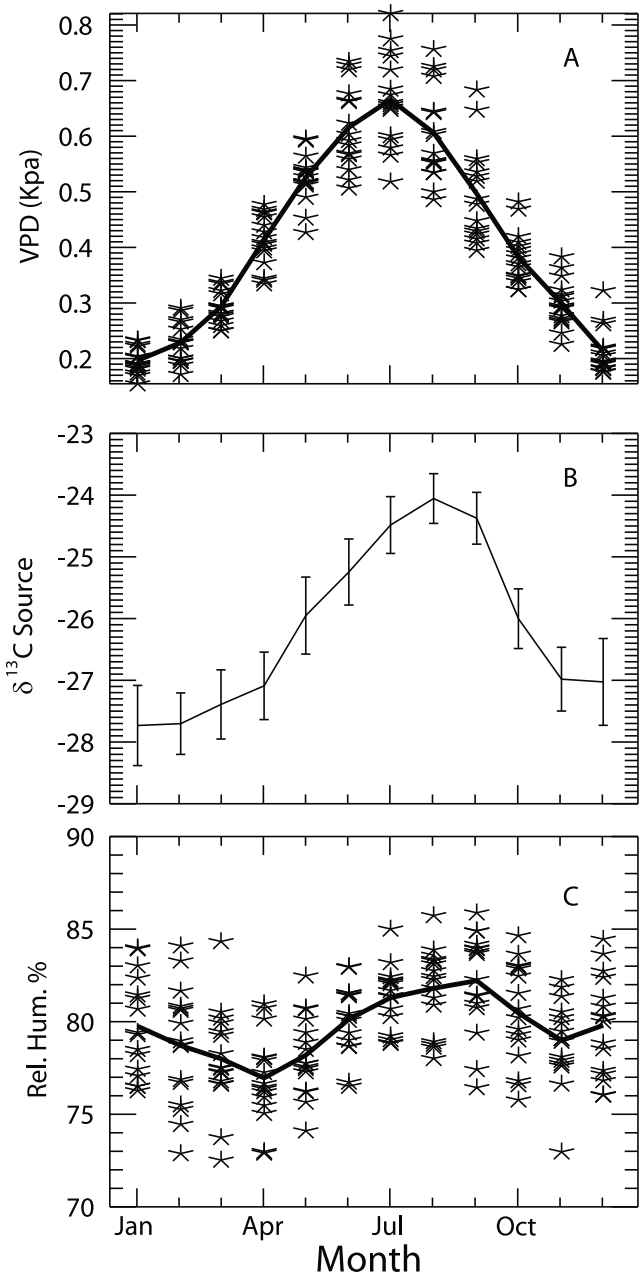

Figure 7. Estimates of seasonal variability in the isotopic signature of source CO_2 (δ_s) compared with different metrics of water vapor in the atmosphere at ITN. The seasonal distribution of (a) vapor pressure deficit (VPD) and (c) relative humidity compared with (b) δ_s calculated from the residuals from the troposphere. VPD was calculated from monthly temperature and relative humidity data from 1990 to 2005 obtained from the North American Regional Reanalysis database (http://www.emc.ncep.noaa.gov/mmb/rreanl/).

physical parameters driving stomatal conductance, respectively in these models, vary proportionally throughout the growing season. Our analysis suggests that the Ball-Berry model for estimating stomatal conductance based on seasonal changes in R may over estimate stomatal conductance and thus isotopic discrimination. In a global analysis of isotopic discrimination, *Suits et al.* [2005] simulated stomatal conductance using the Ball-Berry model embedded in the global SiB 2.5 framework and compared predictions of isotopic discrimination with observations. This analysis revealed consistent agreement between predictions and observations at sites with low D; however, at sites with high D there is much less agreement between predictions and observations with the Ball-Berry model over-predicting stomatal conductance as evidenced by overly depleted values of $\delta^{13}C$ in the biosphere [see *Suits et al.*, 2005, Figure 5]. Based on our analysis we would expect the Leuning model, which explicitly includes D as a physical parameter driving conductance, to provide more accurate predictions of $\delta^{13}C$ in the biosphere at sites with relatively high D.

[40] Although there is generally good agreement between simulated values of δ_{al} and observations from the biosphere and atmosphere suggesting that D is the physical mechanism leading to seasonal isotopic discrimination, there appears to be a one month lag between the peak in simulated values and observed values. This apparent lag is probably due to the physiological response time of the biosphere to changes in atmospheric water vapor. Recent observations from the Pacific Northwest, USA suggest that Δ_{al} inferred from respired air is optimally correlated with D at a time lag of 5 to 10 days [*Bowling et al.*, 2002]. Similarly, a large scale experiment in which trees were girdled documented a 54% reduction in respiration within 1 to 2 months [*Högberg et al.*, 2001]. These findings suggest that the physiology of the biosphere may respond to changing environmental conditions within weeks to months, and thus it is reasonable that the isotopic signature of this physiological response is delayed before being incorporated as cellulose into the biosphere or being detected in the atmosphere.

[41] The spatial extent and temporal importance of the discrepancy between these stomatal conductance models is uncertain from our analysis. If differences in isotopic discrimination between these two stomatal conductance models at the height of the northern hemisphere growth season (approximately 1 to 2 ‰) are widespread across the Southeastern U.S., estimates of net terrestrial carbon uptake for this highly productive region may be very different depending upon the stomatal conductance model employed. Because the subtropical forests of the Southeastern U.S. may constitute up to 30% of the North American carbon sink, or 0.2 Pg C/yr [*Peters et al.*, 2007], identifying and resolving inconsistencies between stomatal conductance models in this region are of critical importance. It is uncertain if this positive temporal covariance of D and R extends into the tropics and, if so, subtle differences in model estimates of stomatal conductance may lead to significant differences in the carbon budget for this highly productive region of the terrestrial biosphere. Previous comparisons between SiB 2.5 simulations and observations have revealed reasonable correspondence between predicted and observed values of δ_{la}, except at sites with high vapor pressure deficit [*Suits et al.*, 2005]. Furthermore, SiB 2.5 failed to capture the full seasonal range of δ_{la} values observed at two sites with observations located within the Amazon [*Ometto et al.*, 2002; *Suits et al.*,

2005]. However, more observations of atmospheric CO_2 and $\delta^{13}CO_2$ are necessary, especially at tropical latitudes, to infer changes in seasonal fluxes and verify model predictions [*Stephens et al.*, 2007]. Even though we have identified temporal differences in the seasonal patterns of isotopic discrimination derived from these two models, these differences may not be apparent when examining annually resolved flux-weighted discrimination. Thus, estimates of flux-weighted discrimination may be different if they are calculated at a monthly time step, rather than an annual time step.

[42] Although all models of stomatal conductance are empirical models, some models may more closely approximate the physical mechanisms driving stomatal conductance. Our observations of carbon isotopes in the biosphere and the overlying troposphere suggest that a model with vapor pressure deficit as the physical mechanism driving stomatal conductance is the most effective model for capturing seasonal variations in the isotopic composition of CO_2 [*Leuning*, 1995]. This is reasonable because the revised stomatal conductance model (equation (13)) proposed by *Leuning* [1995] is effectively a permutation of Fick's law combining equations (9) and (10), with several empirical constants added to account for unexplained biological processes. The main attribute of the Ball-Berry model is its simplicity; with only two empirical parameters that can be readily constrained, it is very amenable to global simulations [*Sellers et al.*, 1996]. However, our results indicate that this model may yield spurious predictions of stomatal conductance on seasonal time scales in environments where D and R are positively covariant through time.

5. Conclusions

[43] We have presented a novel analysis demonstrating that measurements of atmospheric CO_2 and $\delta^{13}CO_2$ can be used to distinguish different fluxes to the atmospheric carbon budget on seasonal time scales. Measurements of $\delta^{13}CO_2$ have been used conventionally to partition the non-fossil portion of the atmospheric CO_2 budget between terrestrial and ocean fluxes on annual time scales. Our residual analysis of seasonal patterns in atmospheric CO_2 and $\delta^{13}CO_2$ suggests that more information about terrestrial processes can be extracted from atmospheric observations on shorter time scales. The observed increase in δ_s during the summer months at the three sites investigated here (UTA, LEF, and ITN) suggests a coherent seasonal pattern of decreased isotopic discrimination by the terrestrial biosphere of North America during the summer months. Although we were not able to explain all of the seasonal variance in sources of CO_2 to the atmosphere, this approach may hold promise for looking at seasonal anomalies in terrestrial carbon fluxes to the atmosphere due to climate variability. Last, we have used isotopic measurements of the atmosphere and biosphere to evaluate how well empirical models of stomatal conductance capture the transfer of carbon and water between the biosphere and the atmosphere. Future climate predictions are predicated on the biosphere's capacity to assimilate a certain fraction of carbon emitted [*Allen et al.*, 2009] and yet the biggest uncertainty in these models is associated with terrestrial processes [*Friedlingstein et al.*, 2006]. As the temperature of the Earth's atmosphere increases in response to CO_2, there will be consequences for the hydrologic cycle [*Held and Soden*, 2006]. Therefore understanding how the biosphere responds to concomitant changes in CO_2, temperature and atmospheric water vapor is critical for predicting the capacity of the terrestrial biosphere to absorb future CO_2 emissions.

[44] **Acknowledgments.** This work benefited from insightful comments from Joe Berry and Graham Farquhar, as well as conversations with Chris Still, Kevin Tu, and David Bowling. We would also like to recognize the members of the Carbon Cycle Group at NOAA/ESRL for assistance during this project. Field assistance was provided by Jeffrey Pippen, and isotopic analyses of cellulose were performed at the Duke Environmental Isotope Laboratory. Estimates of leaf temperature as well as C3 and C4 terrestrial discrimination were provided by Neil Suits, Ian Baker, and Scott Denning. This work would not have been possible without the isotopic data measured and made available by Jim White and Bruce Vaughn at University of Colorado, INSTAAR, as well as sample collectors at NWR, UTA, ITN, and LEF. A.P.B. was supported by a National Research Council Fellowship.

References

Affek, H. P., et al. (2007), Seasonal and diurnal variations of 13C18O16O in air: Initial observations from Pasadena, CA, *Geochim. Cosmochim. Acta*, *71*, 5033–5043, doi:10.1016/j.gca.2007.08.014.

Allen, M. R., et al. (2009), Warming caused by cumulative carbon emissions towards the trillionth tonne, *Nature*, *458*, 1163–1166, doi:10.1038/nature08019.

Bakwin, P. S., et al. (2004), Regional carbon dioxide fluxes from mixing ratio data, *Tellus, Ser. B*, *56*, 301–311, doi:10.1111/j.1600-0889.2004.00111.x.

Bakwin, P. S., et al. (1998), Determination of the isotopic ($^{13}C/^{12}C$) discrimination by terrestrial biology from a global network of observations, *Global Biogeochem. Cycles*, *12*, 555–562, doi:10.1029/98GB02265.

Baldocchi, D. D., and P. C. Harley (1995), Scaling carbon dioxide and water vapour exchange from leaf to canopy in a deciduous forest. II. Model testing and application, *Plant Cell Environ.*, *18*, 1157–1173, doi:10.1111/j.1365-3040.1995.tb00626.x.

Ball, J. T. (1988), An analysis of stomatal conductance, dissertation thesis, 88 pp, Stanford.

Barbour, M. M., et al. (2002), Seasonal variation in del13C and del18O of cellulose from growth rings of Pinus radiata, *Plant Cell Environ.*, *25*, 1483–1499, doi:10.1046/j.0016-8025.2002.00931.x.

Battle, M., et al. (2000), Global carbon sinks and their variability inferred from atmospheric O2 and 13C, *Science*, *287*, 2467–2470, doi:10.1126/science.287.5462.2467.

Bousquet, P., et al. (2000), Regional changes in carbon dioxide fluxes of land and oceans since 1980, *Science*, *290*, 1342–1346, doi:10.1126/science.290.5495.1342.

Bowling, D. R., et al. (2002), 13 C content of ecosystem respiration is linked to precipitation and vapor pressure deficit, *Oecologia*, *131*, 113–124, doi:10.1007/s00442-001-0851-y.

Brendel, O., et al. (2000), A rapid and simple method to isolate pure alpha-cellulose, *Phytochem. Anal.*, *11*, 7–10, doi:10.1002/(SICI)1099-1565(200001/02)11:1<7::AID-PCA488>3.0.CO;2-U.

Ciais, P., et al. (1995), A large Northern Hemisphere terrestrial CO_2 sink indicated by the $^{13}C/^{12}C$ ratio of atmospheric CO_2, *Science*, *269*, 1098–1102, doi:10.1126/science.269.5227.1098.

Conte, M. H., and J. C. Weber (2002), Plant biomarkers in aerosols record isotopic discrimination of terrestrial photosynthesis, *Nature*, *417*, 639–641, doi:10.1038/nature00777.

Conte, M. H., et al. (2003), Molecular and carbon isotopic composition of leaf wax in vegetation and aerosols in a northern prairie ecosystem, *Oecologia*, *135*, 67–77.

DeWar, R. C. (2002), The Ball-Berry-Leuning and Tardieu-Davies stomatal models: Synthesis and extension within a spatially aggregated picture of guard cell function, *Plant Cell Environ.*, *25*, 1383–1398, doi:10.1046/j.1365-3040.2002.00909.x.

Enting, I. G., et al. (1995), A synthesis inversion of the concentration and d13 C of atmospheric CO2, *Tellus*, *47*, 35–52, doi:10.1034/j.1600-0889.47.issue1.5.x.

Falkowski, P., et al. (2000), The global carbon cycle: A test of our knowledge of Earth as a system, *Science*, *290*, 291–296, doi:10.1126/science.290.5490.291.

Farquhar, G. D., et al. (1989), Carbon isotope discrimination and photosynthesis, *Annu. Rev. Plant Physiol.*, *40*, 503–537, doi:10.1146/annurev.pp.40.060189.002443.

Farquhar, G. D., and T. D. Sharkey (1982), Stomatal conductance and photosynthesis, *33*, 317–345.

Flanagan, L. B., et al. (1996), Carbon isotope discrimination during photosynthesis and the isotope ratio of respired CO_2 in boreal forest ecosystems, *Global Biogeochem. Cycles*, *10*, 629–640, doi:10.1029/96GB02345.

Francey, R. J., et al. (1999), A 1000-year high precision record of d13C in atmospheric CO2, *Tellus, Ser. B*, *51*, 170–193, doi:10.1034/j.1600-0889.1999.t01-1-00005.x.

Friedlingstein, P., et al. (2006), Climate-carbon cycle feedback analysis: Results from the C4MIP model intercomparison, *J. Clim.*, *19*, 3337–3353, doi:10.1175/JCLI3800.1.

Fung, I. Y., et al. (1997), Carbon 13 exchanges between the atmosphere and biosphere, *Global Biogeochem. Cycles*, *11*, 507–513, doi:10.1029/97GB01751.

Gleixner, G., et al. (1993), *Correlations Between the 13C Content of Primary and Secondary Plant Products in Different Cell Compartments and That in Decomposing Basidiomycetes*, *Plant Physiol.*, *102*, 1287–1290.

Gruber, N., and C. D. Keeling (2001), An improved estimate of the isotopic air-sea disequilibrium of CO_2: Implications for the oceanic uptake of anthropogenic CO_2, *Geophys. Res. Lett.*, *28*, 555–558, doi:10.1029/2000GL011853.

Gurney, K. R., et al. (2002), Towards robust regional estimates of CO2 sources and sinks using atmospheric transport models, *Nature*, *415*, 626–630, doi:10.1038/415626a.

Held, I. M., and B. J. Soden (2006), Robust responses of the hydrological cycle to global warming, *J. Clim.*, *19*, 5686–5699, doi:10.1175/JCLI3990.1.

Helliker, B. R., et al. (2004), Estimates of net CO_2 flux by application of equilibrium boundary layer concepts to CO_2 and water vapor measurements from a tall tower, *J. Geophys. Res.*, *109*, D20106, doi:10.1029/2004JD004532.

Högberg, P., et al. (2001), Large-scale forest girdling shows that current photosynthesis drives soil respiration, *Nature*, *411*, 789–792, doi:10.1038/35081058.

Hsueh, D. Y., et al. (2007), Regional patterns of radiocarbon and fossils fuel-derived CO_2 in surface air across North America, *Geophys. Res. Lett.*, *34*, L02816, doi:10.1029/2006GL027032.

Katul, G., et al. (2000), Modelling assimilation and intercellular CO_2 from measured conductance: A synthesis of approaches, *Plant Cell Environ.*, *23*, 1313–1328, doi:10.1046/j.1365-3040.2000.00641.x.

Keeling, C. D. (1958), The concentration and isotopic abundances of atmospheric carbon dioxide in rural areas, *Geochim. Cosmochim. Acta*, *13*, 322–334, doi:10.1016/0016-7037(58)90033-4.

Keeling, C. D. (1961), A mechanism for cyclic enrichment of carbon-12 by terrestrial plants, *Geochim. Cosmochim. Acta*, *24*, 299–313, doi:10.1016/0016-7037(61)90024-2.

Krol, M., et al. (2005), The two-way nested global chemistry-transport zoom model TM5: Algorithm and applications, *Atmos. Chem. Phys.*, *5*, 417–432, doi:10.5194/acp-5-417-2005.

Leavitt, S. W., et al. (2002), Spatial expression of ENSO, drought, and summer monsoon in seasonal delta 13 C of ponderosa pine tree rings in southern Arizona and New Mexico, *J. Geophys. Res.*, *107*(D18), 4349, doi:10.1029/2001JD001312.

Leuning, R. (1995), A critical appraisal of a combined stomatal photosynthesis model for C3 plants, *Plant Cell Environ.*, *18*, 339–355, doi:10.1111/j.1365-3040.1995.tb00370.x.

Lloyd, J., and G. D. Farquhar (1994), ^{13}C discrimination during CO_2 assimilation by the terrestrial biosphere, *Oecologia*, *99*, 201–215, doi:10.1007/BF00627732.

Marland, G., et al. (2005), *Global, regional, and national fossil fuel CO_2 emissions*, *Carbon Dioxide Inf. Anal. Cent., Oak Ridge Natl. Lab*, U.S. Dept. of Energy, Oak Ridge, Tenn.

Masarie, K., and P. P. Tans (1995), Extension and integration of atmospheric carbon dioxide data into a globally consistent measurement record, *J. Geophys. Res.*, *100*, 11,593–11,610, doi:10.1029/95JD00859.

Miller, J. B., and P. P. Tans (2003), Calculating isotopic fractionation from atmospheric measurements at various scales, *Tellus, Ser. B*, *55*, 207–214, doi:10.1034/j.1600-0889.2003.00020.x.

Moore, D. J. P., et al. (2006), Annual basal area increment and growth duration of Pinus taeda in response to eight years of free-air carbon dioxide enrichment, *Global Change Biol.*, *12*, 1367–1377, doi:10.1111/j.1365-2486.2006.01189.x.

Ogée, J., et al. (2009), A single-substrate model to interpret intra-annual stable isotope signals in tree-ring cellulose, *Plant Cell Environ.*, *32*, 1071–1090, doi:10.1111/j.1365-3040.2009.01989.x.

Ometto, J., et al. (2002), Carbon isotope discrimination in forest and pasture ecosystems of the Amazon Basin, Brazil, *Global Biogeochem. Cycles*, *16*(4), 1109, doi:10.1029/2001GB001462.

Pataki, D. E., et al. (2003), The application and interpretation of Keeling plots in terrestrial carbon cycle research, *Global Biogeochem. Cycles*, *17*(1), 1022, doi:10.1029/2001GB001850.

Pataki, D. E., et al. (2006), High resolution atmospheric monitoring of urban carbon dioxide sources, *Geophys. Res. Lett.*, *33*, L03813, doi:10.1029/2005GL024822.

Peters, W., et al. (2007), An atmospheric perspective on North American carbon dioxide exchange: CarbonTracker, *Proc. Natl. Acad. Sci. U. S. A.*, *104*, 18,925–18,930, doi:10.1073/pnas.0708986104.

Poussart, P. F., et al. (2004), Resolving seasonality in tropical trees: Multi-decade, high-resolution oxygen and carbon isotope records from Indonesia and Thailand, *Earth Planet. Sci. Lett.*, *218*, 301–316, doi:10.1016/S0012-821X(03)00638-1.

Press, W. H., et al. (1992), *Numerical Recipes in C*, Cambridge Univ. Press, Cambridge, U. K.

Randerson, J. T. (2005), Terrestrial ecosystems and interannual variability in the global atmospheric budgets of $^{13}CO_2$ and $^{12}CO_2$, in *Stable Isotopes and Biosphere Atmosphere Interactions*, edited by L. B. Flanagan et al., pp. 217–234, Elsevier, New York, doi:10.1016/B978-012088447-6/50013-1.

Randerson, J. T., et al. (2001), A possible covariance between terrestrial gross primary production and ^{13}C discrimination: Consequences for the atmospheric 13C budget and its response to ENSO, *Global Biogeochem. Cycles*, *16*, doi:10.1029/2001/GB001845.

Randerson, J. T., et al. (1997), The contribution of terrestrial sources and sinks to trends in the seasonal cycle of atmospheric carbon dioxide, *Global Biogeochem. Cycles*, *11*(4), 535–560, doi:10.1029/97GB02268.

Schimel, D., et al. (2000), Contribution of increasing CO2 and climate to carbon storage by ecosystems in the United States, *Science*, *287*, 2004–2006, doi:10.1126/science.287.5460.2004.

Schlesinger, W. H. (2004), Better living through biogeochemistry, *Ecology*, *85*, 2402–2407, doi:10.1890/03-0242.

Scholze, M., et al. (2003), Climate and interannual variability of the atmosphere-biosphere (CO_2)-C-13 flux, *Geophys. Res. Lett.*, *30*(2), 1097, doi:10.1029/2002GL015631.

Sellers, P. J., et al. (1996), A revised land surface parameterization (SiB2) for atmospheric GCMS. Part I: Model formulation, *J. Clim.*, *9*, 676–705, doi:10.1175/1520-0442(1996)009<0676:ARLSPF>2.0.CO;2.

Stephens, B. B., et al. (2007), Weak northern and strong tropical land carbon uptake from vertical profiles of atmospheric CO_2, *Science*, *316*, 1732–1735, doi:10.1126/science.1137004.

Still, C. J., et al. (2003), Global distributions of C4 photosynthesis, *Global Biogeochem. Cycles*, *17*(1), 1006, doi:10.1029/2001GB001807.

Suits, N. S., et al. (2005), Simulation of carbon isotope discrimination of the terrestrial biosphere, *Global Biogeochem. Cycles*, *19*, GB1017, doi:10.1029/2003GB002141.

Takahashi, T., et al. (2002), Global sea-air CO_2 flux based on climatological surface ocean pCO_2, and seasonal biological and temperature effects, *Deep Sea Res., Part II*, *49*, 1601–1622, doi:10.1016/S0967-0645(02)00003-6.

Tans, P. P. (1980), On calculating the transfer of carbon-13 in reservoir models of the carbon cycle, *Tellus*, *32*, 464–469, doi:10.1111/j.2153-3490.1980.tb00973.x.

Tans, P. P., et al. (1990), Observational constraints on the global atmospheric CO_2 budget, *Science*, *247*, 1431–1438, doi:10.1126/science.247.4949.1431.

Tans, P. P., et al. (1993), Oceanic 13C/12C observations: A new window on ocean CO2 uptake, *Global Biogeochem. Cycles*, *7*, 353–368, doi:10.1029/93GB00053.

Thompson, M. W., and J. T. Randerson (1999), Impulse response functions of terrestrial carbon cycle models: Method and application, *Global Change Biol.*, *5*, 371–394, doi:10.1046/j.1365-2486.1999.00235.x.

Thoning, K. W., et al. (1989), Atmospheric carbon dioxide at Mauna Loa Observatory: 2. Analysis of the NOAA GMCC data, 1974–1985, *J. Geophys. Res.*, *94*, 8549–8565, doi:10.1029/JD094iD06p08549.

Turnbull, J. C., et al. (2006), Comparison of $^{14}CO_2$, CO, and SF 6 as tracers for recently added fossil fuel CO_2 in the atmosphere and implications for biological CO_2 exchange, *Geophys. Res. Lett.*, *33*, L01817, doi:10.1029/2005GL024213.

Wanninkhof, R. (1992), Relationship between wind speed and gas exchange, *J. Geophys. Res.*, *97*, 7373–7382.

Zhang, J., et al. (1995), Carbon isotope fractionation during gas-water exchange and dissolution of CO_2, *Geochim. Cosmochim. Acta*, *59*, 107–114, doi:10.1016/0016-7037(95)91550-D.

Zhou, L., et al. (2006), Long-term record of atmospheric CO_2 and stable isotopic ratios at Waliguan Observatory: Seasonally averaged 1991–2002 source/sink signals, and a comparison of 1998–2002 record to the 11 selected sites in the Northern Hemisphere, *Global Biogeochem. Cycles*, *20*, GB2001, doi:10.1029/2004GB002431.

A. P. Ballantyne, Geological Sciences Department, University of Colorado, Boulder, CO 80309, USA. (ashley.ballantyne@colorado.edu)

J. B. Miller, Cooperative Institute for Research in Environmental Science, University of Colorado, Boulder, CO 80309, USA.

P. P. Tans, NOAA Earth Systems Research Laboratory, Boulder, CO, USA.